displacement regardless of the direction, the lattice at this location is thus annealed substantially, as if the effective L_r is reduced to $L_r^{\mathrm{eff}} \approx L_r I_{\mathrm{dc}}/I_{\mathrm{ac}}$. Thus, at very small biases, the disordered phase is present only within x_d^{ad} from the edges, as in the absence of a bias, where the disordered vortices leave and re-penetrate every cycle. Vortices that drift deeper into the bulk under the influence of I_{dc} are practically fully annealed because of the very short L_r^{eff}. As a result, the initial decrease of R_{ac} up to $I_{\mathrm{dc}} \approx 2\,\mathrm{mA}$ (see Fig. 4a) is relatively small. The corresponding $J_{\mathrm{ac}}(x)$ in Fig. 4b at $I_{\mathrm{dc}} = 1.7\,\mathrm{mA}$ shows narrow contaminated regions near the edges, very similar to the zero-bias case in Fig. 2. However, as I_{dc} is increased, L_r^{eff} grows and the bulk of the sample becomes contaminated by the penetrating disordered vortex phase, leading to a marked drop of R_{ac}. In this situation, $J_{\mathrm{ac}}(x)$ at $I_{\mathrm{dc}} = 5.7\,\mathrm{mA}$ shows a wide region of disordered phase at the left edge. When I_{dc} is inverted to $-5.7\,\mathrm{mA}$, a similar situation is observed, but now the vortices—and hence the disordered phase—penetrate from the right edge, as expected.

The revealed mechanism readily explains a wide range of additional reported phenomena. (1) The history of the previously applied current is encoded in the spatial profile of the lattice disorder, which is preserved after the current is switched off owing to negligible thermal relaxation. On reapplying the current, the vortex system will display a memory of all the parameters of the previously applied current, including its direction, duration, amplitude and frequency, as observed experimentally[13,14]. (2) Application of a current step $I < I_c^{\mathrm{dc}}$ to a sample in the ordered vortex phase results in a transient response which decays to zero, as the disordered phase is able to penetrate only a limited distance. The resulting new I_c of the sample is given by the condition that $I_c = I$, as derived by fast transport measurements[14,15]. Such transient phenomena would also display characteristic times shorter than, or comparable to, the vortex transit time across the sample, in agreement with observations[13,14]. (3) The competition between the contamination and annealing processes is expected to result in local instabilities, causing the reported noise enhancement below the peak effect[1,2] (see also Fig. 4a). (4) Related phenomena should be observed in high-temperature superconductors in the vicinity of the peak effect associated with the melting transition, or near the second magnetization peak, consistent with experiments[3–6,12,16]. (5) In high-temperature superconductors there is an additional consideration of thermal activation of vortices over the surface barriers, which may explain the reported slow voltage oscillations[3–6]. If the thermal activation rate is higher than, or comparable to, the driving rate, the slowly injected lattice will be ordered, in contrast to the disordered vortex phase injected at higher drives. Thus, at a given applied current, if the bulk of the sample is in the ordered vortex phase, much of the current flows on the edges, rapidly injecting a disordered vortex phase through the surface barrier. Once the bulk becomes contaminated, the resulting slower vortex motion again causes injection of an ordered phase. This feedback mechanism can explain the voltage oscillations[3,6] in $YBa_2Cu_3O_7$ and similar narrow-band noise[4,5] in $YBa_2Cu_3O_7$ and $Bi_2Sr_2CaCu_2O_8$ with characteristic frequencies comparable to the inverse transit time. Last, we note that the described phenomena should be absent in the Corbino disk geometry where vortices do not cross the sample edges. Our studies of $NbSe_2$ in this geometry (Y.P. *et al.*, manuscript in preparation) confirm this prediction. ☐

Received 5 August; accepted 16 November 1999.

1. Marley, A. C., Higgins, M. J. & Bhattacharya, S. Flux flow noise and dynamical transitions in a flux line lattice. *Phys. Rev. Lett.* **74,** 3029–3032 (1995).
2. Merithew, R. D. *et al.* Persistent metastable states in vortex flow at the peak effect in $NbSe_2$. *Phys. Rev. Lett.* **77**, 3197–3199 (1996).
3. Kwok, W. K. *et al.* Dynamic instabilities in the vortex lattice of $YBa_2Cu_3O_7$. *Physica C* **293,** 111–117 (1997).
4. D'Anna, G. *et al.* Vortex-motion-induced voltage noise in $YBa_2Cu_3O_7$ single crystals. *Phys. Rev. Lett.* **75,** 3521–3524 (1995).
5. Tsuboi, T., Hanaguri, T. & Maeda, A. Local density fluctuations of moving vortices in the solid and liquid phases in $Bi_2Sr_2CaCu_2O_8$. *Phys. Rev. Lett.* **80**, 4550–4553 (1998).
6. Gordeev, S. N. *et al.* Current-induced organization of vortex motion in type-II superconductors. *Nature* **385,** 324–326 (1997).
7. Bhattacharya, S. & Higgins, M. J. Flux-flow fingerprint of disorder: melting versus tearing of a flux-line lattice. *Phys. Rev. B* **52,** 64–67 (1995).
8. Henderson, W. *et al.* Metastability and glassy behavior of a driven flux-line lattice. *Phys. Rev. Lett.* **77,** 2077–2080 (1996).
9. Banerjee, S. S. *et al.* Anomalous peak effect in $CeRu_2$ and $2H$-$NbSe_2$: Fracturing of a flux line lattice. *Phys. Rev. B* **58,** 995–999 (1999).
10. Banerjee, S. S. *et al.* Metastability and switching in the vortex state of $2H$-$NbSe_2$. *Appl. Phys. Lett.* **74,** 126–128 (1999).
11. Wordenweber, R., Kes, P. H. & Tsuei, C. C. Peak and history effect in two-dimensional collective flux pinning. *Phys. Rev. B* **33,** 3172–3180 (1986).
12. Kokkaliaris, S. *et al.* Onset of plasticity and hardening of the hysteretic response in the vortex system of $YBa_2Cu_3O_{7-\delta}$. *Phys. Rev. Lett.* **82**, 5116–5119 (1999).
13. Henderson, W., Andrei, E. Y. & Higgins, M. J. Plastic motion of a vortex lattice driven by alternating current. *Phys. Rev. Lett.* **81,** 2352–2355 (1998).
14. Xiao, Z. L., Andrei, E. Y. & Higgins, M. J. Flow induced organization and memory of a vortex lattice. *Phys. Rev. Lett.* **83,** 1664–1667 (1999).
15. Andrei, E. Y. *et al.* Current driven organization of magnetic vortices. *J. Phys. IV* **10,** 5–10 (1999).
16. Metlushko, V. *et al.* Driven vortex states and relaxation in single crystal $YBa_2Cu_4O_8$. Preprint cond-mat/9804121 at ⟨http://xxx.lanl.gov⟩ (1999).
17. Gammel, P. L. *et al.* Structure and correlation of a flux line lattice in crystalline Nb through peak effect. *Phys. Rev. Lett.* **80,** 833–836 (1998).
18. Khaykovich, B. *et al.* Vortex-lattice phase transitions in $Bi_2Sr_2CaCu_2O_8$ crystals with different oxygen stoichiometry. *Phys. Rev. Lett.* **76,** 2555–2558 (1996).
19. Giamarchi, T. & Le Doussal, P. Elastic theory of pinned flux lattices. *Phys. Rev. Lett.* **72,** 1530–1533 (1994).
20. Ertas, D. & Nelson, D. R. Irreversibility, mechanical entanglement and thermal melting in superconducting vortex crystal with point impurities. *Physica C* **272,** 79–85 (1996).
21. Vinokur, V. *et al.* Lindemann criterion and vortex-matter phase transitions in high-temperature superconductors. *Physica C* **295,** 209–217 (1998).
22. Pardo, F. *et al.* Topological defects in the flux-line lattice and their relationship to the critical current of a type-II superconductor. *Phys. Rev. Lett.* **78,** 4633–4636 (1996).
23. Yaron, U. *et al.* Structural evidence for a two-step process in the depinning of the superconducting flux-line lattice. *Nature* **376,** 753–755 (1995).
24. Bean, C. P. & Livingston, J. D. Surface barrier in type-II superconductors. *Phys. Rev. Lett.* **12,** 14–16 (1964).
25. Paltiel, Y. *et al.* Surface barrier dominated transport in $NbSe_2$. *Phys. Rev. B* **58,** R14763–R14766 (1998).
26. Fuchs, D. T. *et al.* Transport properties governed by surface barriers in $Bi_2Sr_2CaCu_2O_8$. *Nature* **391,** 373–376 (1998).
27. Fuchs, D. T. *et al.* Possible new vortex matter phases in $Bi_2Sr_2CaCu_2O_8$. *Phys. Rev. Lett.* **80,** 4971–4974 (1998).
28. Burlachkov, L., Koshelev, A. E. & Vinokur, V. M. Transport properties of high-temperature superconductors: surface vs. bulk effect. *Phys. Rev. B* **54,** 6750–6757 (1996).

Acknowledgements

We thank P. B. Littlewood for discussions. The work at the Weizmann Institute of Science was supported by the Israel Science Foundation—Centre of Excellence Program, by the US-Israel Binational Science Foundation (BSF), and by the Alhadeff research award. E.Y.A. was supported by the NSF.

Correspondence and requests for materials should be addressed to Y.P.
(e-mail: hpalt@wis.weizmann.ac.il).

Singularity dynamics in curvature collapse and jet eruption on a fluid surface

Benjamin W. Zeff*, Benjamin Kleber*, Jay Fineberg† & Daniel P. Lathrop*

* *Institute for Plasma Research and Department of Physics,*
The University of Maryland, College Park, Maryland 20742, USA
† *The Racah Institute of Physics, The Hebrew University of Jerusalem, Jerusalem, Israel*

Finite-time singularities—local divergences in the amplitude or gradient of a physical observable at a particular time—occur in a diverse range of physical systems. Examples include singularities capable of damaging optical fibres and lasers in nonlinear optical systems[1], and gravitational singularities[2] associated with black holes. In fluid systems, the formation of finite-time singularities

cause spray and air-bubble entrainment[3], processes which influence air–sea interaction on a global scale[4,5]. Singularities driven by surface tension have been studied in the break-up of pendant drops[6–9] and liquid sheets[10–12]. Here we report a theoretical and experimental study of the generation of a singularity by inertial focusing, in which no break-up of the fluid surface occurs. Inertial forces cause a collapse of the surface that leads to jet formation; our analysis, which includes surface tension effects, predicts that the surface profiles should be describable by a single universal exponent. These theoretical predictions correlate closely with our experimental measurements of a collapsing surface singularity. The solution can be generalized to apply to a broad class of singular phenomena.

In our experiment, surface singularities are produced by the collapsing depressions of standing waves, a phenomenon first observed by Longuet-Higgins[13]. A cylindrical tank, partially filled with a fluid, is vertically oscillated with an acceleration of the form $a(t) = A\sin(\omega t)$, where A is the acceleration amplitude, and ω is the driving frequency. This forcing, known as Faraday excitation, generates subharmonic standing waves on the fluid surface[14]. Below a critical standing wave height h_c the fluid surface topology remains smooth and simply connected. Above h_c, the collapsing wave entrains an air bubble beneath the surface and changes its topology from simply to multiply connected. Thus, the critical height represents the threshold of the surface topology change. At this point, where parameter values are just below those values for which droplet entrainment occurs, the resulting inertial collapse creates a singularity on the fluid surface at which the velocity and surface curvature diverge. This singularity focuses the kinetic energy of the fluid along the central axis and produces a narrow, high-speed vertical jet (Fig. 1). Experimentally, we observe the approach to this singularity; as with many such systems, an ultraviolet cutoff exists which prevents a full divergence of the physical variables. In this case, viscous forces[15] become important near in time and space to the singularity and provide one source for this cutoff. In addition, the Rayleigh instability in the jet causes the formation of a droplet at the tip and eventually causes the jet to break into droplets.

In order to simplify nearly intractable nonlinear equations, the fluid is assumed to be irrotational and incompressible, and the air above the fluid is considered to be of zero density. Near the location of the event, the surface tension forces, kinetic energy density, and acceleration are all thought to diverge jointly, and gravity may safely

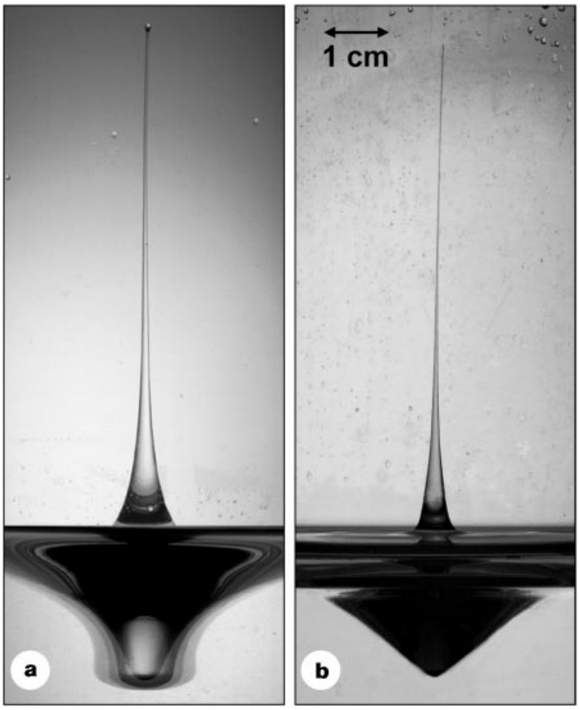

Figure 1 Surface wave collapses and resulting jets. **a**, A composite of two photographs showing the collapse of a surface wave depression and the subsequent upward jet caused by self-focusing of the kinetic energy associated with a near singularity. The singularities are produced in a cylindrical tank with an inner diameter of 12.7 cm filled to a depth of 6.5 cm with a glycerin–water solution with a viscosity of 1.94 cm^2 s^{-1}. A sinusoidal signal of frequency 7.84 Hz generated by computer controls a servo circuit driving the linear actuator which holds the tank. Initially, the system is driven at a low amplitude, 2.39 m s^{-2}, which sets up a repeatable periodic standing wave. Once the wave state settles into a periodic state, the driving amplitude is increased suddenly at a zero crossing to 3.23 m s^{-2} (or nearby values to produce different wave states), after which the height of the standing waves increases with each subsequent period. Once the standing wave is sufficiently tall, it produces a deep depression which collapses to a singularity and jet. Images of the developing singularity and jet are captured with a 2,000 × 3,000 pixel digital camera and a five-flash array which are triggered via computer signal and a digital delay generator. With this system, five exposures separated in time by as little as 250 μs can be captured on a single image. Here, the first photograph is a four-exposure image and shows four time steps of the collapse which correspond to 8 ms, 4 ms, 2 ms, and 1 ms before the singularity. The second photograph shows the jet 33 ms after the singularity. **b**, A second composite, here at a viscosity of 0.26 cm^2 s^{-1}. The driving frequency and amplitude are 8.00 Hz and 4.64 m s^{-2}, respectively. The conical shape of the surface at the time of the singularity is shown with a resultant jet. In **a**, viscous effects provide an ultraviolet cutoff which smoothes the asymptotic cone.

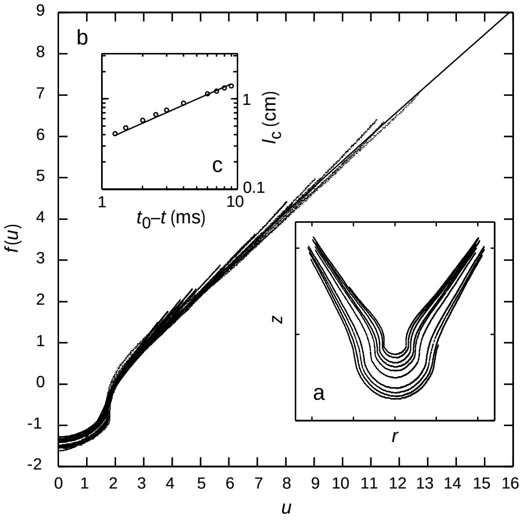

Figure 2 Comparison of theoretical and experimental surface profiles for 0.26 cm^2 s^{-1} glycerin–water solution. **a**, The surface profile of a collapsing depression at ten times before the singularity: 9 ms, 8 ms, 7 ms, 6 ms, 4 ms, 3 ms, 2.5 ms, 2 ms, 1.5 ms, and 1.25 ms. Curves closer to the central axis occur alter in time. The base of depression accelerates upward and reaches the origin at the time t_0. The standing wave which produces this depression is subcritical in height, so it collapses to a near singularity. The surface profiles are converted from digital images to coordinates and corrected for the refraction caused by the cylindrical tank. The height of the waves and qualitative information about the events are determined from images captured by a 250 frames/second video camera. **b**, The theoretical form of the surface profile, calculated numerically as described in the text for We = 4,000, is shown as a solid line. The asymptotic cone angle is $\theta = 60°$. The points are the ten surface profiles from **a** scaled according to the similarity solution. The profiles collapse into one self-similar form which agrees well with theory. Because of a viscous ultraviolet cutoff, overhang begins to develop in the surface profiles at late times (<1 ms). This overhang is not present in the numerical form. **c**, A log–log plot of l_c, the mean distance from the origin to all points (with $f(u) < 0$, where $f(u) = h(r, t)(t_0 - t)^{-2/3}$ is the scaled height of the fluid surface) along a given profile, and $(t_0 - t)$ for each of the curves in **a** and **b**. The solid line represents the predicted two-thirds scaling law.

be neglected. An important result of these assumptions is that the physical forcing of the system no longer enters into the local equations of motion. Hence, the same equations describe the curvature collapse and singularities in many other systems with free surfaces, independent of forcing, including spherical and cylindrical cavitation bubble collapse, droplet impact rebounds and, by considering the gravity-dominated case, wave impact and jets on a sheer wall. We show that the inclusion of surface tension not only expands on previous work[6,17], but is also responsible for the selection of a universal solution describing jet formation in collapsing cavities. The system can be described by three equations, one for the bulk and two at the air–fluid interface: the Laplace equation representing incompressibility, the kinematic equation for the fluid surface, and the Bernoulli equation at the fluid surface. These three equations in cylindrical coordinates are, respectively:

$$\nabla^2 \phi = 0 \tag{1}$$

$$\frac{\partial h}{\partial t} + \frac{\partial h}{\partial r}\frac{\partial \phi}{\partial r} = \frac{\partial \phi}{\partial z} \tag{2}$$

$$\frac{\partial \phi}{\partial t} + \frac{1}{2}(\nabla \phi)^2 + \frac{\sigma}{\rho}\left(\frac{1}{R_1} + \frac{1}{R_2}\right) = 0 \tag{3}$$

Here ϕ is the velocity potential ($\boldsymbol{v} = \nabla\phi$), z is the axial coordinate ($z = h$ at the free surface), r is the radial distance, σ and ρ are the surface tension and density of the fluid, respectively, and R_1 and R_2 are the principal radii of curvature of the surface.

There is no formal mathematical framework for attacking such a system of nonlinear partial differential equations. However, in past analysis of singularities[6,7,18,19], a similarity method has proven an effective tool. We postulate a power-law scaling in times close to the singularity:

$$h(r,t) = (t_0 - t)^{\alpha} f[r(t_0 - t)^{\beta}] \tag{4}$$

$$\phi(r,z,t) = (t_0 - t)^{\gamma} g[r(t_0 - t)^{\beta}, z(t_0 - t)^{-\alpha}], \tag{5}$$

in which t_0 is the time of the singularity. The variables r and z have been scaled by the characteristic length and velocity scales l and v, and t has been scaled by a characteristic time $t = l/v$. This scaling yields a single non-dimensional parameter, the Weber number $\mathrm{We} = \rho v^2 l/\sigma$ that governs the dynamics of the collapse. Physically, We is the ratio of the kinetic energy of the fluid motion to the surface energy that contains the fluid. We estimate the Weber number based on the height of the last smooth wave h and the velocity $v = h\omega/2$ (where $\omega/2$ is the angular frequency of the wave).

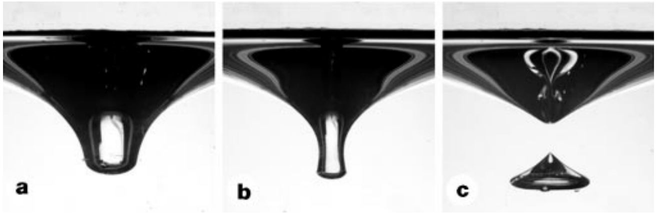

Figure 3 Surface depressions produced by surface waves of three different heights in 1.94 $\mathrm{cm}^2\,\mathrm{s}^{-1}$ fluid. **a**, The depression produced by a collapsing wave of subcritical height, $h < h_c$. The surface topology remains smooth and simply connected. A jet is produced with a tip velocity of 7 $\mathrm{m\,s}^{-1}$. **b**, The depression produced by a standing wave with $h \approx h_c$. The walls are nearly vertical, and no bubble is entrained. This state produces a very narrow jet with a velocity of 30 $\mathrm{m\,s}^{-1}$. **c**, The depression produced by a standing wave with $h > h_c$. A large conical bubble is produced as the topology changes from simply to multiply connected. The curvature is singular at the point of bubble pinch-off. The bubble decreases the kinetic energy of this jet, which has a velocity of 6 $\mathrm{m\,s}^{-1}$. Large bubble oscillations and concomitant emitted sound account for much of the energy loss. Each of these photographs was taken at the same time relative to the phase of the forcing.

For a similarity solution to exist, the time-dependence of all terms in equations (1)–(3) must be the same. Substituting equations (4) and (5) and requiring the time-dependence to be identical in each term, we find that only a single value is allowed for each of the exponents: $\alpha = 2/3$, $\beta = -2/3$, and $\gamma = 1/3$. These exponents were also found by Keller and Miksis[10] in their analysis of a breaking liquid sheet and apply to all cases when only surface tension and inertial forces are dominant. This result differs significantly from the case in which surface tension is neglected[16,17], in which, for given conditions, a continuous family of exponents is possible with no well defined selection criterion.

We can infer important characteristics of the singularity from the values of the scaling exponents, including the profile of the fluid surface near in time to the singularity. As $t_0 - t \rightarrow 0$, the scaled radius in the argument of f diverges. Since $\alpha = -\beta$, the function f must be linear in its argument for times near the singularity in order for the height to remain finite. Near the singularity, then, the height of the surface is linear with respect to the radius; that is, $h(r,t) \rightarrow Cr$ and the surface is a cone as $t \rightarrow t_0$ (Fig. 1b). Numerical evidence indicates that only certain values of the cone angle $C = \cot\theta$ (the angle of the surface off the vertical) are allowed. The system is now described by three partial differential equations for f and g in the scaled radius $u = r(t_0 - t)^{-2/3}$ and height $v = z(t_0 - t)^{2/3}$.

$$\nabla^2 g = 0 \tag{6}$$

$$-\frac{2}{3}f + \frac{2}{3}u\frac{\partial f}{\partial u} + \frac{\partial f}{\partial u}\frac{\partial g}{\partial u} = \frac{\partial g}{\partial v} \tag{7}$$

$$-\frac{1}{3}g + \frac{2}{3}u\frac{\partial g}{\partial u} + \frac{2}{3}f\frac{\partial g}{\partial v} + \frac{1}{2}\left(\frac{\partial g}{\partial u}\right)^2 + \frac{1}{2}\left(\frac{\partial g}{\partial v}\right)^2 + \frac{1}{\mathrm{We}}\left(\frac{1}{R_1} + \frac{1}{R_2}\right) = 0 \tag{8}$$

To solve equations (7) and (8) numerically and find a form for the surface profile (Fig. 2b), we write equation (6) as a series of known solutions to the Laplace equation with unknown coefficients:

$$g = c_{1/2} r_s^{1/2} P_{1/2}(\cos\theta) + c_{-1} r_s^{-1} + c_{-2} r_s^{-2} P_1(\cos\theta) + \ldots \tag{9}$$

in which r_s is the spherical radius from the centre of the collapsing cone, θ is the polar angle, and P_n are Legendre polynomials. Asymptotic analysis of equation (8) requires the leading-order behaviour to be $r_s^{1/2}$. In solving for $f(u)$ numerically, the coefficients in the above series and the angle θ_0 at large radius are assigned values. This form of g is substituted into equation (2) which is then integrated to determine $f(u)$. The coefficients and angle are varied, and $f(u)$ and $g(u,v)$ are recalculated iteratively until equation (3) is satisfied. This numerical form predicts not only the shape of the collapsing surface in our experiment, but due to the lack of a specific forcing in equations (6)–(8), is a general form which describes any axisymmetric surface singularity dominated by inertia and surface tension.

We experimentally observe the approach to the singularity in the curvature collapse of the surface profile of the fluid surface. Figure 3 shows three collapsing surface depressions in a 1.94 $\mathrm{cm}^2\,\mathrm{s}^{-1}$ fluid in the tank, one subcritical, one nearly critical, and one beyond the critical height. The collapse of all three of these surfaces would produce a fluid jet. Figure 3b shows the collapse of the depression near the critical point which produces a energetic singularity. The walls of the depression collapse radially inward while the bottom of the depression accelerates upward toward an origin. At the point of singularity, the velocities from equation (5) are predicted to diverge. Figure 4 details this dependence experimentally. If we vary the forcing such that the last smooth standing wave approaches the amplitude h_c—the value above which we observe bubble

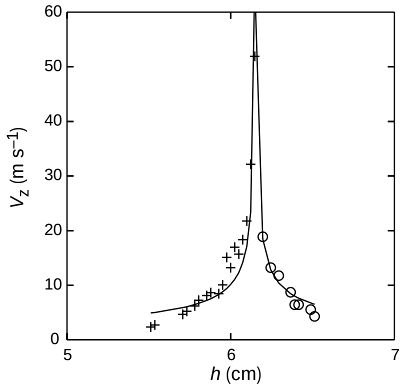

Figure 4 Dependence of jet velocity on surface wave height for 1.94 cm^2 s^{-1} fluid. The velocity of the jet tip depends strongly on the height of the last smooth standing wave before the singularity. The tip velocity increases rapidly as $h \rightarrow h_c$. The bubble formation (for $h > h_c$) requires energy, and the tip velocity decreases sharply with increasing bubble size. Near $h = h_c$, jet tip velocities exceeding 52 m s^{-1} have observed. This velocity dependence is consistent with the Weber number We of the jet being derived from that of the last smooth wave. The solid line is the functional form $\rho v_z^2(h - h_c)/\sigma = \mathrm{We}$ where ρ is the fluid density, v_z is the jet tip velocity, and σ is the surface tension. Tip velocities are found by observing the shadow of the jet tip. A vertical HeNe laser sheet passes horizontally through the tank through the central axis and shines on two phototransistors separated by a vertical distance of 2.7 cm. As the jet moves upward through the laser sheet, the curved droplet tip refracts the light and forms a shadow. Using a digital oscilloscope, the time delay between the appearance of the shadow on the two phototransistors is measured, and the velocity of the tip obtained. The high-viscosity fluid simplifies these measurements by damping out small-scale perturbations on the surface and creating smooth, vertical jets.

entrainment to first occur—the velocity peaks sharply, reaching values higher than 52 m s^{-1}. The entrainment of even very small bubbles decreases the jet velocity significantly.

We now analyse the surface profile of a subcritical collapsing depression—a near singularity. Each curve in Fig. 2a represents the shape of the surface profile at a given time before the singularity. We scale these data according to the similarity solution, using the location of the origin to which the profiles collapse vertically and the time of the singularity as parameters. Figure 2b shows the result of this scaling superimposed on the numerical solution. It is clear that the numerical solution is in good agreement with the observed surface profiles, indicating that the analysis captures the behaviour of the system. The collapse of the experimental data is consistent with a two-thirds scaling exponent, though for late times, an ultraviolet cutoff due to viscous effects causes increasing deviation from the self-similar form. When the fluid velocity becomes sufficiently large as the singularity is approached, viscous forces can no longer be neglected, and the above analysis would need to be extended to include rotation. Experimentally, overhang in the surface profile is seen to develop, suggesting that the fluid is not irrotational. As the fluid velocity is increased, the viscous ultraviolet cutoff also results in systematic rounding of the asymptotic cone. These viscous effects can be decreased by using a fluid with lower viscosity. However, in low-viscosity fluids, small-scale structures are observed on the standing waves before the collapse. Although we observe curvature collapse and jets in water (viscosity 0.01 cm^2 s^{-1}), parasitic capillary waves and other perturbations complicate these surface profiles and make them difficult to analyse.

In most previous applications of similarity solutions, the original partial differential equations reduced to ordinary differential equations. However, in this work, our system reduces to partial differential equations—a more difficult, but tractable, situation[9,10]. This method can now be applied to such problems as sheet-like jets erupting from fluid surfaces, as is seen in wave breaking on a cliff[20] in the gravity-dominated case. A power-law scaling for the form of the fluid jets produced in our experiments by the surface curvature collapse is also known[21]. One challenge remaining is to match the solution discussed here regarding the collapsing depression before the singularity with the known behaviour of the jet after the singularity. In addition, further study of the viscous ultraviolet cutoff very close in time to the singularity is needed, and it would also be of interest to investigate the dependence of solutions on the Weber number. ☐

Received 25 March; accepted 11 November 1999.

---

1. Shen, Y. R. *The Principles of Nonlinear Optics* (Wiley, New York, 1984).
2. Weinberg, S. *Gravitation and Cosmology* (Wiley, New York, 1972).
3. Newell, A. C. & Zakharov, V. E. Rough sea foam. *Phys. Rev. Lett.* **69,** 1149–1151 (1992).
4. Hoffman, P. F., Kaufman, A. J., Halverson, G. P. & Schrag, D. P. A neoproterozoic snowball earth. *Science* **281,** 1342–1346 (1998).
5. Sarmiento, J. L. & Le Quere, C. Oceanic carbon dioxide uptake in a model of century-scale global warming. *Science* **274,** 1346–1350 (1996).
6. Eggers, J. & Dupont, T. F. Drop formation in a one-dimensional approximation of the Navier-Stokes equation. *J. Fluid Mech.* **262,** 205–221 (1994).
7. Eggers, J. Universal pinching of 3D axisymmetric free surface flow. *Phys. Rev. Lett.* **71,** 3458–3460 (1993).
8. Brenner, M. *et al.* Breakdown of scaling in droplet fission at high Reynolds number. *Phys. Fluids* **9,** 1573–1590 (1997).
9. Day, R. F., Hinch, E. J. & Lister, J. R. Self-similar capillary pinchoff of an inviscid fluid. *Phys. Rev. Lett.* **80,** 704–707 (1998).
10. Keller, J. B. & Miksis, M. J. Surface tension driven flows. *SIAM J. Appl. Math.* **43,** 268–277 (1983).
11. Hou, T. Y., Lowengrub, J. S. & Shelley, M. J. The long-time motion of vortex sheets with surface tension. *Phys. Fluids* **9,** 1933–1954 (1997).
12. Chen, Y.-J. & Steen, P. H. Dynamics of inviscid capillary breakup: collapse and pinchoff of a film bridge. *J. Fluid Mech.* **341,** 245–267 (1997).
13. Longuet-Higgins, M. S. Bubbles, breaking waves and hyperbolic jets at a free surface. *J. Fluid Mech.* **127,** 103–121 (1983).
14. Faraday, M. On a peculiar class of acoustical figures, and on certain forms assumed by groups of particles on vibrating elastic surfaces. *Phil. Trans R. Soc. Lond.* **121,** 299–340 (1831).
15. Boulton-Stone, J. M. & Blake, J. R. Gas bubbles bursting at a free surface. *J. Fluid Mech.* **254,** 437–466 (1993).
16. Longuet-Higgins, M. S. & Oguz, H. N. Critical microjets in collapsing cavities. *J. Fluid Mech.* **290,** 183–201 (1995).
17. Longuet-Higgins, M. S. & Oguz, H. N. Critical jets in surface waves and collapsing cavities. *Phil. Trans. R. Soc. Lond. A* **355,** 625–639 (1997).
18. Barenblatt, G. I. *Scaling, Self-similarity, and Intermediate Asymptotics* (Cambridge University Press, 1996).
19. Zakharov, V. E. in *Breaking Waves.* (eds Banner, M. L. & Grisham, R. H. J.) (Springer, Berlin, 1992).
20. Cooker, M. J. & Peregrine, D. H. Violent surface motion as near-breaking waves meet a wall. In *Breaking Waves.* (eds Banner, M. L. & Grisham, R. H. J.) (Springer, Berlin, 1992).
21. Hogrefe, J. E. *et al.* Power-law singularities in gravity-capillary waves. *Physica D* **123,** 183–205 (1998).

Acknowledgements

We thank R. Rohde, M. Brenner, A. Bertozzi, J. Drake, T. Antonsen, E. Ott and J. Pyle for their input. D.P.L. is a Cottrell Scholar of the Research Corporation. This work was supported by the National Science Foundation.

Correspondence and requests for materials should be addressed to D.P.L.
(e-mail: dpl@complex.umd.edu).